DESIGN SENSITIVITY STUDIES ON THE T-TAIL FLUTTER OF A TRANSPORT AIRCRAFT

N.G. Vijaya Vittala*, A.C. Pankaj* and D. V. Venkatasubramanyam*

Abstract

The studies of dynamic and aeroelastic characteristics of a high T-Tail transport aircraft at component and full level using MSC/NASTRAN code and correlation with the results obtained from ground vibration tests of the aircraft have thrown light on the complexities of the T-Tail dynamics and flutter characteristics. The critical flutter velocities of the complete aircraft have been evaluated by the PK and KE methods of NASTRAN. The effects of variability of the locations and magnitude of the non-structural masses in the fuselage on the T-Tail flutter velocities have been studied by a parametric analysis. Sensitivity study of the elevator mass balancing on its dynamics and the flutter velocities have also been addressed. The flutter velocities and margins have been examined from the certification aspects. Addressing design issues of the aircraft related to fuselage flexibility and T-Tail flutter from an aeroelastic point of view has been attempted in this paper.

***Keywords**: T-Tail Flutter, Aircraft Flutter, Transport Aircraft dynamics/Flutter, Certification, T-Tail Design*

Nomenclature

b	= reference semi-chord
q	= dynamic pressure
B_s	= modal damping matrix
F_s	= generalized unsteady force vector
K_s	= generalized stiffness matrix
M_s	= generalized mass matrix
Q_{hh}	= modal aerodynamic damping matrix
U	= true air velocity
ρ	= air density
ξ	= generalized displacement vector

Abbreviation

CG	= Centre of Gravity
ER	= Elevator Rotation
HT	= Horizontal Tail
FLB	= Fuselage Longitudinal Bending
MAC	= Mean Aerodynamic Chord

Introduction

The interactions of a flexible structure with the aerodynamic forces acting on it are severe enough to influence its structural and aerodynamic design. The dynamic and aeroelastic analysis of an aircraft with main reference to its lifting and control surfaces is an essential aspect in the finalization of the design cycle, for obtaining flight clearance and certification of the aircraft [(1,2]. The aircraft under consideration is a twin turbo prop, multi-role, light transport aircraft having a cantilevered low wing and a high T-Tail, rear-fuselage mounted pusher engines, with a maximum takeoff weight of 7100 kg and seating capacity of 14 passengers. The landing gear is of retractable tri-cycle type configuration. The aircraft has a pressurized cabin and is designed to have high cruise speed, high specific range and short take off and landing distances.

Dynamic and flutter characteristics of the aircraft have been studied at the component level and at the integrated level, using NASTRAN code. The finite element model has been fine tuned to the results obtained from the ground vibration tests after the first cut analysis. The design dive speed for the aircraft being 145.28 m/sec, the flutter critical velocity has to be 1.15 times the dive speed, so as to satisfy the certification requirements as stipulated in FAR 25. A parametric study of the T-Tail flutter has been conducted to relate the natural frequencies and flutter

* Scientist, Structural Technologies Division, National Aerospace Laboratories (A Constituent Establishment of Council of Scientific Industrial Research, Rafi Marg, New Delhi), Bangalore-560 017, India, Email : acpankaj@nal.res.in
Manuscript received on 26 Aug 2009; Paper reviewed and accepted as a Full Lengh Contributed Paper on 30 Nov 2009

velocity of the aircraft with some sensitive parameters like the magnitude and placement of the non-structural masses in the fuselage, fuel weights in the wing and remedial mass balance on the elevator.

Geometry and Finite Element Model

The Fuselage is all metallic, semi monocoque structure, circular in cross section, designed to accommodate a stand up cabin. The wing is all metallic with large aspect ratio, spar rib construction with port and starboard wings permanently joined at the centerline. It has on its either side a trailing edge outboard carbon composite aileron and two flaps and is suspended from the fuselage at four points located at the front and the rear spars, two points each on port and starboard side at a distance of 0.6m from the aircraft centerline. At the intersection of spar center and the aircraft central line a drag link is present. A fuel tank and a landing gear well are also accommodated in the wing. The horizontal stabilizer is a single piece, two spars all metallic construction attached to the fin by four bolts. It has a plain flap-type spar-rib structured elevator consisting of two halves interconnected by a torque tube and a universal joint. The port elevator has a balance tab and the starboard elevator has a servomotor-operated trim tab. The elevator with tabs is mass balanced about its hinge line. The elevator is hinged to the horizontal tail at four points and actuated through a torque tube attached to the control circuit. The vertical tail has a fin and a rudder. The fin is all-metallic with a 3-spar construction. The spars are permanently attached to the fuselage by extending them into a torque box, which is inside the rear fuselage. The vertical tail has an all-composite rudder of spar rib construction attached to the tail at three hinge points. The rudder has two tabs; one is the follow up balance tab and the other an electronically actuated trim tab operated by a servomotor. A torque tube attached to the control circuit actuates the rudder.

The fuselage, control surfaces, the stub wing and the stress- cleared model of the wing have been used for the dynamic analysis. The finite element model was generated using Quad4 and Tria3 shell elements of MSC/NASTRAN [3]. The bolts at the attachment points are modeled by bar and rigid elements. The horizontal tail with elevator is attached to the vertical tail with rudder to form the high T-Tail configuration of the aircraft. The attachments have been simulated using rigid elements. Appropriate multipoint constraints have been applied to simulate the motion of control surfaces. The necessary modifications have been done on these finite element models for updating the non-structural masses including the balance masses and the stiffness of the actuating mechanisms for the control surfaces. The individual FE component models were checked for their mass, centre of gravity details and then integrated together to realize FE model of the full aircraft, (Fig.1). Convergence analysis for the size and number of elements have been carried out on the component models and integrated to realize model of the aircraft. The final integrated aircraft model consisted of more than 6, 72,000 degrees of freedom. A close correlation for the mass and centre of gravity of an aircraft configuration with an overall weight of 5575 kg and fuel weight of 250 kg can be seen for the finite element model and design values (Table-1).

Aerodynamic Model

The aerodynamic mesh model of the complete aircraft consists of flat panels for the lifting surfaces and a combination of slender and interference bodies for the fuselage and engine nacelles (Fig.2). The mesh for all the lifting surfaces has been idealized by means of trapezoidal boxes that lie parallel to flow direction. Care has been taken to avoid overlap at attachment points and hinge lines, to provide finer mesh at leading edge, to ensure alignment of boxes along the hinge line and to include wing tips as well. All the lifting surfaces are defined under the same aerodynamic interference group. Surface spline functions have been used to generate the necessary interpolation matrix to estimate the displacement of aerodynamic grids based upon the displacement of structural grids. Bodies like fuselage, engine nacelle, external stores etc are idealized as "slender" and "interference" elements. The primary purpose of the slender body elements is to account for the forces arising from the motion of the body, whereas the interference elements are used to account for the interference effects among all bodies and panels in the same group. Shorter interference elements are placed in regions of substantial interference, e.g., near the wing-fuselage

Table-1 : Comparison of Mass and CG Values

Design Mass (Kg)	Centre of Gravity Location (mm)			FEM Mass (Kg)	Centre of Gravity Location (mm)		
	X	Y	Z		X	Y	Z
5575.14	7929.71	0.0	0.0	5572.14	7926.68	-5.640	-24.09

intersection. Bodies are classified as y, z, or zy depending on the type of motion allowed in the y, z or both the directions.

The right and left wing surfaces have been divided into four main zones corresponding to the main wing, inboard and outboard flaps and aileron. These zones have been subdivided depending on the chord and span. In total the right half of the wing has two hundred and sixty-one boxes. Similarly the left half of the wing has two hundred and sixty-one boxes making a total of five hundred and twenty-two boxes. The horizontal tail has been divided into three main surfaces corresponding to horizontal stabilizer, elevator and tabs. Horizontal tail in total has one hundred and seventy six boxes. The three surfaces of the vertical tail i.e., fin; rudder and tabs have been suitably subdivided into trapezoidal boxes. Vertical tail in total has seventy-four boxes. The symmetric stub wing surfaces has chord wise four and span wise five divisions and twenty boxes in total in each wing. The fuselage of the aircraft has been modeled as a zy slender body consisting of a series of elements having half-widths equal to the cross-sectional radii at each bulkhead station to ultimately realize the fuselage contour. To account for aerodynamic interference between panels and bodies, the interference tube has been defined with its half-width equal to the maximum cross-sectional radius of the body (fuselage). The two nacelles have been modeled as zy slender bodies with slender body elements and interference elements. The interference elements have identical half-widths equal to the maximum nacelle radius. A beam spline has been used to interpolate between aerodynamic and structural displacements for both fuselage and nacelles.

The aerodynamic meshes described above are integrated thereafter to realize the aerodynamic model of the major individual components and the full aircraft. The interference between the body (fuselage) and the lifting surfaces like wing, horizontal tail, vertical tail and stub wing have been taken into consideration by declaring interference groups.

Analysis

Dynamic Analysis

Dynamic analysis of the free-free aircraft has been carried out with no constraints at the wing attachment points [4]. Appropriate condition for the nested position of flaps, hinge condition for the three control surfaces and respective control circuit stiffness have been applied to them at the actuation points for the initial analysis. In all the subsequent analyses the control surfaces torsional stiffness have been fine-tuned to realize the rotational modes of the elevator and rudder frequencies obtained through the Ground Vibration Tests (GVT) of the aircraft. The dynamic frequency spectrum of the complete aircraft has been obtained by invoking the Lanczos method in NASTRAN with unit mass criteria for normalizing the mode shapes.

Ground Vibration Test

GVT system had 4 electrodynamic modal shakers with a force rating of 220 N and a maximum frequency rating of 2000 Hz, acquiring excitation force signals from 4 force transducers and structural response from 56 accelerometers. Data acquisition was done by a 60 channel LMS SCADAS III system with a signal conditioning unit. The Modal test and analysis software resident on Intel Pentium IV PC communicates with the SCADAS system by a SCSI connection card. Due to limitations in the data acquisition system, the response measurements were limited to maximum 56 locations at any instant. Therefore these had to be relocated after each set of acquisition and the data acquisition had to be carried out in 2 or 3 segments. The aircraft tires were deflated to 50% pressure to simulate the free-free condition approximately. The exciter locations were selected in such a way that it excited the entire aircraft to capture all the modes of interest. One shaker was placed on the right and left wing tips respectively, one on the horizontal tail leading edge and one on a fuselage bulkhead. A Signal generator with 50% burst random signal, frequency bandwidth of 100Hz and resolution of 0.2 Hz. was deployed in exciting all the 4 shakers simultaneously through power amplifiers and measured signals were displayed on the host computer screen for viewing signal acquisition and overload information. Time domain signals of both, force transducers and response accelerometers were also monitored online. 50 averages of time responses were used to obtain noise free signal response. Uniform window was applied to both excitation and response signals. The frequency response function and coherence were monitored and checked before acquiring the final data. This procedure was repeated to measure response at all locations. The data collected was processed to get the desired modal characteristics.

Flutter Analysis

In the flutter solutions, full finite element aircraft model has been used. The structural frequencies and modal vectors obtained from the Eigen value solution have

been used for the subsequent flutter analysis in NASTRAN. The structure is assumed to undergo harmonic oscillations and the generalized equation of motion for flutter in the frequency domain is given by:

$$\left(-\omega^2 \left[M_s \right] + i\,\omega \left[B_s \right] + \left[K_s \right] \right) \left\{ \xi\,(i\,\omega) \right\} = \left\{ F_s\,(i\,\omega) \right\} \tag{1}$$

The generalized unsteady force F_s ($i\omega$) is also expressed as :

$$\left\{ F_s\,(i\,\omega) \right\} = q \left[Q_{hh}\,(ik) \right] \left\{ \xi\,(i\,\omega) \right\} \tag{2}$$

The generalized unsteady aerodynamic force matrix is complex and are calculated for user-defined values (at a given mach number) of the reduced frequency $k = \omega\, b/U$, and the dynamic pressure q = (1/2) ρU^2. The flutter analysis of the aircraft has been carried out by taking the first 45 modes into consideration, up to 56 Hz of the spectrum. The cut off frequency includes rotational modes of the control surfaces, fuselage bending modes, bending and torsion modes of the lifting surfaces, which are susceptible for flutter. The velocity range considered for the analysis starts from 70 m/sec to 300 m/sec in steps of 10 m/sec. The PK and KE methods have been used for the flutter solutions of both the configurations. The principal advantage of the PK-method is that it produces results directly for given values of velocity, whereas the KE-method requires iteration to determine the reduced frequency for flutter. In addition, the damping obtained by the PK method is a more realistic estimate of the physical damping than the artificial damping used in the KE method, which is a mathematical artifice.

Sensitivity Studies

In the parametric study the correlation of the magnitudes and placement of the non-structural masses in the fuselage on the prominent natural frequencies affecting the T-Tail and flutter velocity of the aircraft have been studied. Thus the effect of fuselage flexibility [5] on the horizontal tail bending modes and elevator rotation has been considered and the studies have been carried out for the following cases:

Case 1: Different payload cases necessitates relocations of the non structural masses in the fuselage, as such the locations of the non structural masses in the fuselage have been varied from the most forward to aft C.G., ie. 24.32% to 35.88% of MAC respectively, for an aircraft configuration with an overall weight of 7100 kg.

Case 2: The study is repeated for Case 1, with a reduction of fuel weight of 235 kg in the wing leading to an overall weight of 6865 kg for the aircraft.

Case 3: A fraction of the non-structural mass (40 kg) in the fuselage has been reduced and a corresponding increase of 20 kg of fuel weight in each wing has been effected maintaining the same overall weight of 7100 kg and centre of gravity as in Case 1.

Case 4: For an aircraft configuration of case1 with a centre of gravity at 24.32% MAC, a fraction of the fuel weight in the wing has been removed and a corresponding increase has been done on the non-structural mass in the rear end of the fuselage, maintaining the same overall aircraft weight of 7100 kg. The values of the fuel weights reduced in the wing and the corresponding increase done on the non-structural mass at the rear end of the fuselage has resulted in a C.G travel of the aircraft from 28.55% to 39.30% MAC.

Finally a sensitivity study has been carried out varying the balance mass on the elevator from 0.4 to 1.6 kg in steps of 0.4 kg, for an aircraft configuration of Case 1 and Case 2 with a centre of gravity at 35.88% MAC, co-relating its effects on the flutter velocity of the aircraft.

Results and Discussion

The results of the dynamic analysis for the aircraft configuration with overall weight of 5575 kg and fuel weight of 250 kg for the modes of significant importance are presented in Table- 2 and Fig.3. The free-free analysis of the aircraft results in clear six rigid body modes followed by the elastic modes. The rigid body mode frequencies are less than 0.1 Hz. The frequencies of the translation modes are much lower than that of the rotational modes. The pure rotational mode of the rudder occurs at 7.12 Hz after the first few elastic modes of wing. The wing first symmetric bending (Fig.3a) occurs at 6.27 Hz and first anti-symmetric bending with fuselage rotation (5.12 Hz) modes are followed by rudder rotation and lower stub wing / yoke modes. The elevator rotational mode (Fig.3b) takes place at 11.03 Hz. The wing bending and torsion modes are well separated. The major effect of presence of high horizontal tail in the T-Tail configuration is seen in the occurrence of horizontal tail bending and in-plane modes prior to vertical tail lateral bending. Coupling of

Table-2 : Dynamic Results of the Aircraft (5575 Kg, X-C.G = 7926.68 mm = 29.34% MAC)

Mode No.	Frequency (Hz)	Remarks	Mode No.	Frequency (Hz)	Remarks
1	9.117E-5	X-Translation	17	13.52	Fuselage Torsion (Wing 2nd Asym + HT Inplane)
2	1.601E-4	Y-Translation	18	15.05	VT + Fuselage Longitudinal + HT Sym. Bending + Elevator Rotation
3	5.592E-4	Z-Translation	22	17.83	Stubwing inplane
4	1.088E-2	Pitching	23	18.55	Wing 2nd Asym. Bending
5	1.136E-1	Rolling	24	20.83	HT 1st Sym. Bending
6	3.110E-1	Yawing	25	22.21	Aileron Sym. Rotation
7	5.124	Wing 1st Asymmetric bending	26	22.22	Aileron Asym. Rotation
8	6.274	Wing 1st Symmetric bending	30	27.00	Fuselage Lateral Bending
9	7.053	1st Asymmetric bending of horizontal tail (HT) + Rudder rotation	31	32.58	Fuselage longitudinal bending (out and in board flaps Sym. bending)
10	7.123	Rudder rotation	33	34.47	In board flaps symmetric bending
11	7.483	Yoke Sym (Wing 1st Sym. Bending + VT Lateral + HT Asym. Bending)	35	39.80	Out board flap symmetric bending
12	7.817	Yoke Asym (Wing 1st Sym. Bending + VT Lateral + HT Asym. Bending)	44	53.01	Wing Asym. Torsion + (Flaps Asym. Bending)
13	8.396	Stubwing Sym. Bending (Wing 1st Sym. B+VT Trans)	45	54.69	Wing Sym. Torsion (Flaps Asym. Bending)
14	10.56	Wing in-plane mode (horizontal tail asym. bending)	60	67.82	Horizontal Tail Asymmetric Torsion
15	11.03	Elevator rotation	61	68.41	Horizontal Tail SymmetricTorsion
16	11.39	VT Lateral Bending + 1st Asym. Bending of HT	80	99.59	Vertical Tail Torsion

symmetric modes of lifting surfaces with longitudinal movement of fuselage, as also that of anti-symmetric modes with the lateral movement has been observed. Fig.3c shows the vertical tail longitudinal mode associated with horizontal tail symmetric bending and fuselage bending in the XZ-plane. Distinct stub wing and / or yoke modes occur at 7.48 Hz, 17.8 Hz. The effect of the engine mass attached to the yoke is seen in the occurrence of stub wing lateral mode before the fore-aft mode. The role of in-plane stiffness of the wing, horizontal tail and vertical tail is seen in the occurrence of symmetric in-plane modes. The symmetric bending of horizontal tail (Fig.3d) occurs at 20.83 Hz. The aileron has both symmetric and anti-symmetric rotational modes, which are quite close. The symmetric aileron rotational mode occurs at 22.21 Hz, after the wing second bending mode. Fuselage lateral and longitudinal bending modes are quite high at 27.0 Hz and 32.58 Hz respectively. Fuselage torsion occurs much later. The flap modes lie between 30 and 41 Hz and the wing torsion mode in the range of 51 Hz. The inboard and out board flaps modes are well separated. Further the inboard and out board flaps of the port and starboard side have separate symmetric and anti-symmetric modes. A few shell modes of the fuselage are seen thereafter followed by higher modes of lifting and control surfaces. Horizontal tail symmetric torsion and asymmetric torsion occurs at frequencies of 68.41Hz and 67.82 Hz respectively. Vertical tail torsion occurs at 99.59 Hz.

Table-3 compares the dynamic frequencies obtained through finite element analysis of the aircraft with the ground vibration test results. A good correlation between the analysis and experimental results are seen. The flutter results obtained through NASTRAN are presented in Table-4. The flutter plots are shown in Fig.4. The coupled mode (Fig.3c) of fuselage longitudinal bending with the horizontal tail symmetric bending and elevator rotation leads to flutter.

The results of parametric sensitivity studies conducted for various cases with particular reference for the modes involved in leading to the flutter of the aircraft have been tabulated in Table-5 to Table-8. These studies have revealed that the variation in the fuel mass results in marginal changes in the wing frequencies, where as the variation in the nonstructural mass distribution in the fuselage results in changes in fuselage longitudinal mode frequencies. However the increase in the aircraft mass due to either of these variations results in decrease in the HT symmetric bending frequency. This is due to coupling of symmetric modes of the lifting surfaces with longitudinal movement of the fuselage, as also that of the anti-symmetric modes with the lateral movement. The same trends are observed for the fuselage longitudinal and HT symmetric bending modes with the aircraft CG traveling from front to rear. A careful examination of the coupling of symmetric modes of the HT with longitudinal movement of the fuselage has shown that their movements are out of phase with each other, resulting in decreased rigidity of the HT joint explaining the decrease in HT symmetric mode frequency with increase in the fuselage longitudinal bending and vice versa. The plots of the separation of fuselage bending and elevator rotation frequency and flutter velocity with variation in centre of gravity of the aircraft presented show identical trends (Fig.5 and 6). This leads to the identification of the frequency separation between the fuselage longitudinal bending and elevator rotation as a sensitive parameter for the flutter velocities of the aircraft. The decrease in fuel weights (Case 4) for the aircraft and

Table-3 : Ground Vibration Test Results (5575 Kg, X-C.G = 7926.68 mm = 29.34% MAC)

Mode Remarks	GVT		FEM
	Freq. (Hz)	Damping (%)	Freq. (Hz)
Wing 1st Asymmetric Bending	5.65	1.167	5.124
Wing 1st Symmetric Bending	6.85	1.641	6.274
Coupled Mode (HT Asymmetric Bending + VT Lateral	7.43	0.849	7.483
Stub Wing Symmetric Bending	7.89	1.227	8.396
HT 1st Asymmetric Bending	10.57	1.629	10.56
Elevator Rotation	11.02	3.05	11.03
VT Lateral Bending (HT 1st Asymmetric Bending)	11.52	0.852	11.39
Coupled Mode (Wing 2nd Asymmetric + HT Inplane)	14.09	2.159	13.52
VT + Fuselage Longitudinal + HT Symetric Bending + Elevator Rotation	15.85	1.19	15.05
Wing 2nd Asymmetric Bending	18.87	0.747	18.55
HT 1st Symmetric Bending	21.97	0.768	20.83
Aileron Symmetric Rotation	27.68	0.622	22.21
Wing 2nd Symmetric Bending (Fuselage Bending)	26.38	1.326	24.97
Tab Mode	33.84	1.529	-
Elevator Asymmetric Rotation	39.44	1.685	-

Table-4 : Flutter Analysis of the Aircraft (5575 Kg, X-C.G = 7926.68 mm = 29.34% MAC)

Method	Mode No.	Flutter Velocity (m/s)	Flutter Frequency (Hz)
PK	18	176.98	14.34
KE	18	177.47	14.339

Table-5 : Comparison of Frequencies (Hz) for Case 1

X-C.G (% MAC)	HT Symm. Bending	HT Asym. Bending	18th Mode	VT Lateral Bending	Fus. Long Bending	Elevator Rotation	Flutter Vel. (m/sec)
24.32	18.54	9.67	13.82	11.26	29.859	11.0284	118.48
28.21	18.51	9.71	13.91	11.27	30.218	11.0284	123.69
30.15	18.49	9.73	13.96	11.27	30.386	11.0284	126.57
32.1	18.48	9.75	14.01	11.28	30.544	11.0284	129.67
35.88	18.44	9.79	14.08	11.29	30.741	11.0284	136.11

Table-6: Comparison of Frequencies (Hz) for Case 2

X-C.G (% MAC)	HT Symm. Bending	HT Asym. Bending	18th Mode	VT Lateral Bending	Fus. Long Bending	Elevator Rotation	Flutter Vel. (m/sec)
24.32	18.98	9.67	13.96	11.26	29.95	11.028	121.905
28.21	18.96	9.71	14.06	11.27	30.361	11.028	126.91
30.15	18.95	9.73	14.10	11.27	30.552	11.028	129.69
32.1	18.94	9.75	14.15	11.28	30.734	11.028	132.64
35.88	18.90	9.79	14.23	11.29	30.968	11.028	138.76

Table-7: Comparison of Frequencies (Hz) for Case 3

X-C.G (% MAC)	HT Symm. Bending	HT Asym. Bending	18th Mode	VT Lateral Bending	Fus. Long Bending	Elevator Rotation	Flutter Vel. (m/sec)
24.32	18.53	9.67	13.81	11.26	29.821	11.0283	117.071
28.21	18.50	9.71	13.90	11.27	30.161	11.0283	122.319
30.15	18.48	9.73	13.94	11.28	30.318	11.0283	125.219
32.1	18.47	9.75	14.0	11.28	30.465	11.0283	128.349
35.88	18.42	9.79	14.06	11.29	30.644	11.0283	134.909

Table-8: Comparison of Frequencies (Hz) for Case 4

X-C.G (% MAC)	HT Symm. Bending	HT Asym. Bending	VT+Fus. Long. Mode	VT Lateral Bending	Fus. Long Bending	Elevator Rotation	Flutter Vel. (m/sec)
28.55	18.58	9.66	13.68	11.26	29.819	11.027	116.17
31.39	18.65	9.65	13.62	11.26	29.778	11.027	114.4
34.90	18.68	9.64	13.56	11.25	29.713	11.027	113.07
39.30	18.69	9.62	13.52	11.25	29.622	11.027	113.18

Table-9: Comparison of Frequencies (Hz) with Additional Balance Mass (Case 1 - 35.88% MAC)

Balance Mass (Kg)	HT Symm. Bending	HT Asym. Bending	VT+Fus. Long. Mode	VT Lateral Bending	Fus. Long Bending	Elevator Rotation	Flutter Vel. (m/sec)
0.4	18.44	9.79	14.07	11.28	30.725	10.947	168.11
0.8	18.44	9.79	14.07	11.28	30.7165	10.867	285.15
1.2	18.44	9.79	14.06	11.28	30.704	10.789	Divergence
1.6	18.44	9.79	14.06	11.28	30.692	10.712	Divergence

Table-10: Comparison of Frequencies (Hz) with Additional Balance Mass (Case 2 - 35.88% MAC)

Balance Mass (Kg)	HT Symm. Bending	HT Asym. Bending	VT+Fus. Long. Mode	VT Lateral Bending	Fus. Long Bending	Elevator Rotation	Flutter Vel. (m/sec)
0.4	18.90	9.79	14.22	11.29	30.956	10.946	168.74
0.8	18.90	9.79	14.21	11.28	30.943	10.866	539.43
1.2	18.90	9.79	14.21	11.28	30.931	10.788	Divergence
1.6	18.90	9.79	14.20	11.28	30.919	10.711	Divergence

corresponding increase of non-structural weights at the rear end of the fuselage results not only in the aircraft CG travel to the rear but also in decrease in fuselage longitudinal bending frequencies. This is owing to the fact that unlike Case 1 to Case 3, the relative mass as compared to the fuselage stiffness increases with the addition of extra masses at the rear end, and in such a condition, the frequency separation (FLB-ER) reduces, leading to reduction of flutter velocities.

The studies of increase in balance mass of the elevator are presented in Table-9 and Table-10. The increase of balance masses on the elevator naturally has resulted in decrease in the elevator rotational frequency but has no significant effect on the HT symmetric bending frequency. However the frequency separation between the fuselage longitudinal bending and elevator rotation is a sensitive parameter for the flutter velocities of the aircraft showing a steady increase as seen in Fig.7. The flutter velocity is so sensitive to the additional mass balance such that, it varies linearly in the beginning and then increases almost exponentially leading to high divergence speeds instead of flutter (Fig.8).

VT longitudinal mode which is coupled with HT symmetric bending, elevator rotation and fuselage longitudinal bending (18th Mode) also shows marginal decrease with the aircraft CG travel from aft to rear. For this critical mode, the phase angle between a node on the HT and a corresponding node in the same span wise location on the elevator tip have been evaluated from the complex eigen vectors of flutter analysis results. Fig.9 shows an exponential curve fit of the same indicating a rapid increase in the flutter velocity for low values of this parameter. However the relative difference in the real eigen vectors for the same points obtained from the normal modes analysis interestingly shows the same trend as illustrated in Fig.10. This implies that the magnitude of the flutter velocity of a configuration is latent in the relative movement of the horizontal stabilizer and the elevator.

Conclusions

- The dynamic characteristics of the aircraft established by analytical and experimental methods and the flutter characteristics obtained by PK and KE methods show a good correlation. The flutter velocity and the flutter frequency obtained by the PK method in NASTRAN are 176.98 m/sec and 14.34 Hz (Table-4), as against the critical flutter velocity of 167.07 m/sec, having an adequate margin from certification aspects.

- The T-Tail construction is a complicated configuration from the dynamic and flutter point of view. The in plane modes are almost accompanied by an out-of-plane motion. Flutter results indicate that the coupled mode of horizontal tail symmetric bending combined with the fuselage and vertical tail longitudinal bending and elevator rotation goes to flutter. The participation of the

aft fuselage flexibility is seen in the occurrence of this coupled mode.

- Different payload cases necessitating relocations of the non structural masses in the fuselage resulting in the CG travel to the rear the aircraft or reduction in quantum of fuel in turn reducing the overall aircraft weight without the CG variation results in increase in the flutter velocities.

- The addition of non-structural weights in the rear end with minor aircraft CG travel to the rear end decreases the flutter velocities, even if the fuel weights are reduced.

- The aircraft flutter velocity is quite sensitive to the additional mass balance on the elevator which reduces the elevator rotational frequency, increasing its separation from the fuselage longitudinal mode resulting in increased flutter velocities.

- The finding that the magnitude of the flutter velocity of a configuration is latent in the relative movement of the horizontal stabilizer and the elevator, obtained from the real eigen vectors in normal modes analysis interestingly, can be operated as a design tool leading to a great deal of time saving for the designer to estimate the approximate flutter speed during the initial design iteration stages.

- The out of phase in plane mode of the fuselage with the coupled symmetric modes of the HT, has a bearing on the rigidity of the HT joint, not only necessitating the attention of the designer on the joint stiffness at the initial design stage but also demanding attention for its inspection during the maintenance cycles of the aircraft.

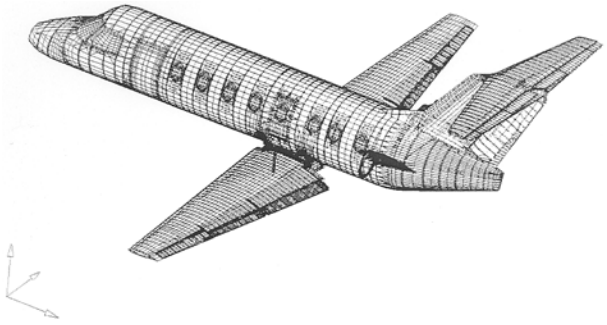

Fig.1 Finite Element Model of the Aircraft

Acknowledgements

The authors acknowledge all the support received from colleagues of different groups in the laboratory. The authors are grateful to the Director, National Aerospace Laboratories, Bangalore, India, for his kind permission to publish the paper.

References

1. Fowler, S.B., "Flutter Analysis of X33", AIAA Paper No: 2000-1589, 2000.

2. FAR 25 Aviation Regulations, 2000.

3. MSC/NASTRAN Documentation (Msc Software Corporation, USA), 2005.

4. Vijaya Vittala N.G., Pankaj, A.C. and Swarnalatha, R., "Dynamic and Aeroelastic Analysis of a Transport Aircraft", International Conference on Aerospace Technologies, Bangalore, India, 2008.

5. Washizu, K., "A Note on the T-Tail Flutter", RAE-LT No.1546, 1971.

6. Scanlan, R.H. and Rosenbaum, R., "Introduction to the Study of Aircraft Vibration and Flutter", The Macmillan Company, New York, 1996.

7. Bisplinghoff, R. and Ashley, H., "Principles of Aeroelasticity", Dover Phoenix Editions, New York, 1962.

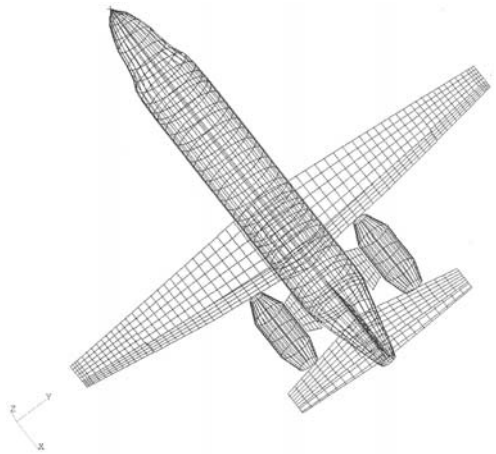

Fig.2 Aerodynamic Model of the Aircraft

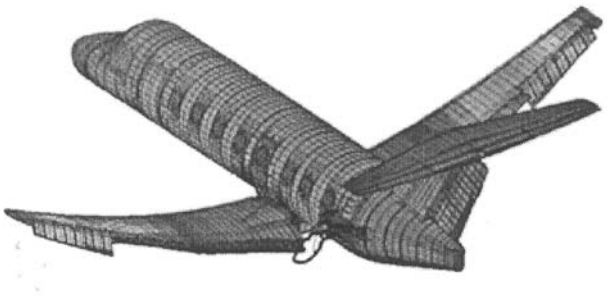

Fig.3a Wing 1st Symmetric Bending (6.274 Hz)

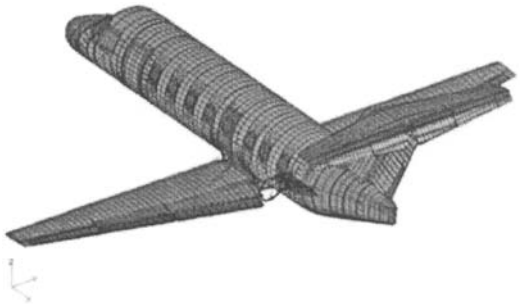

Fig.3b Elevator Rotation (11.03 Hz)

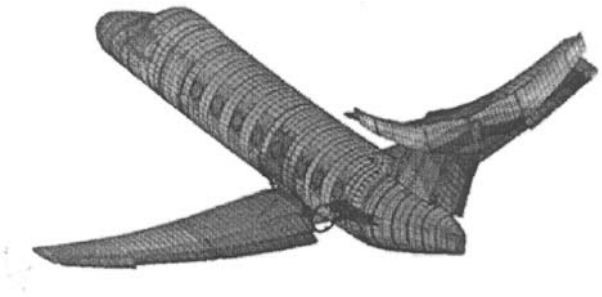

Fig.3c Fuselage + VT Longitudinal + HT Symmetric Bending + Elevator Rotation (15.05 Hz)

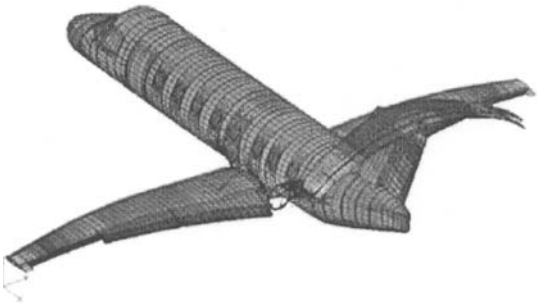

Fig.3d HT 1st Symmetric Bending (20.83 Hz)

Fig.3 Mode Shapes of the Aircraft

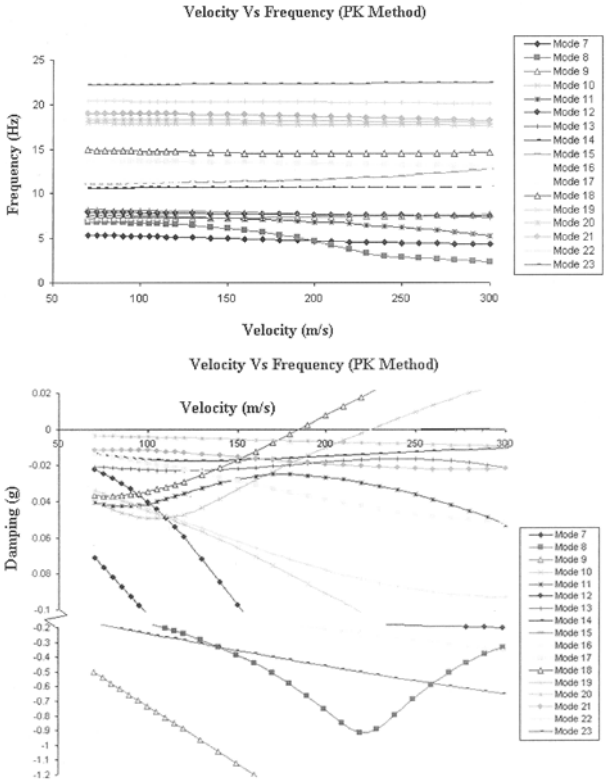

Fig.4 Flutter Plots of the Aircraft (5575 Kg, X-CG = 7926.68 m = 29.34% MAC)

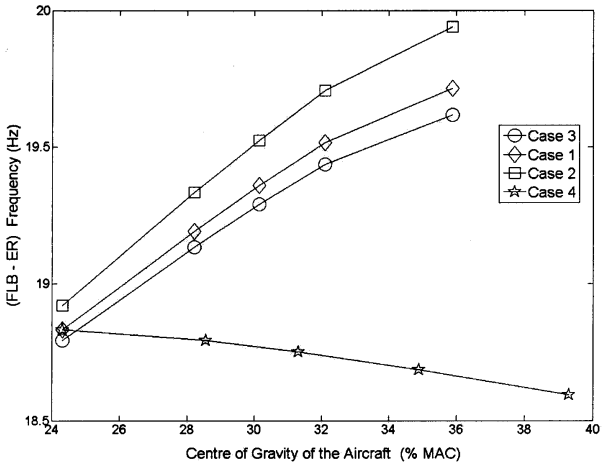

Fig.5 Variation of Frequency Separation with Centre of Gravity of Aircraft

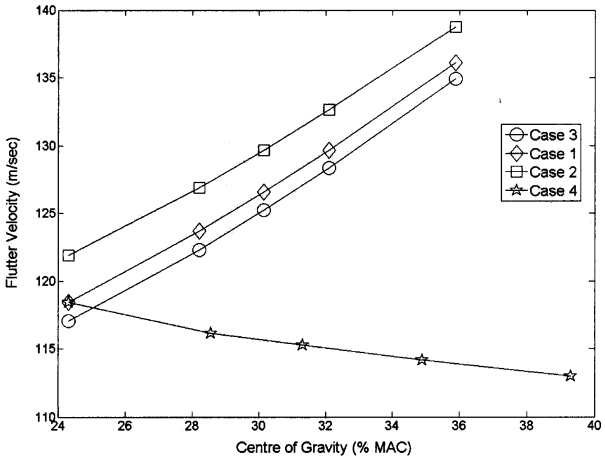

Fig.6 Variation of Flutter Velocity with Centre of Gravity of Aircraft

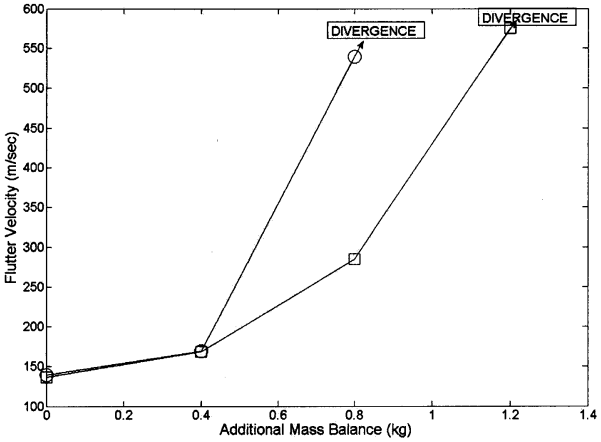

Fig.8 Variation of Flutter Velocity with Additional Mass Balance on the Elevator

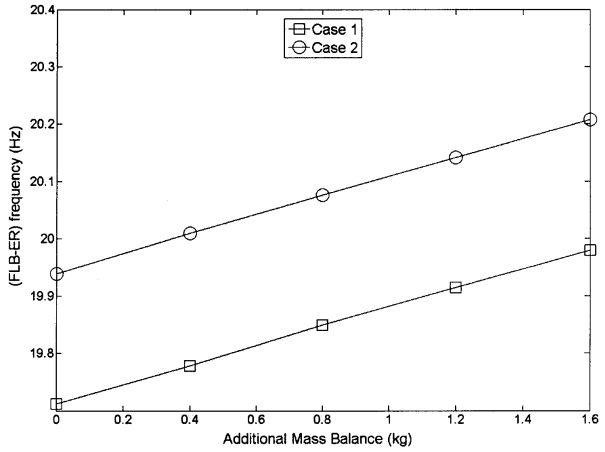

Fig.7 Variation of Frequency Separation with Additional Mass Balance on the Elevator

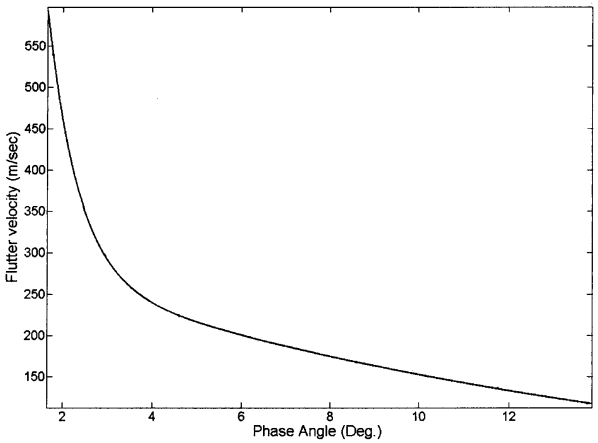

Fig.9 Variation of Flutter Velocity with Phase Angle

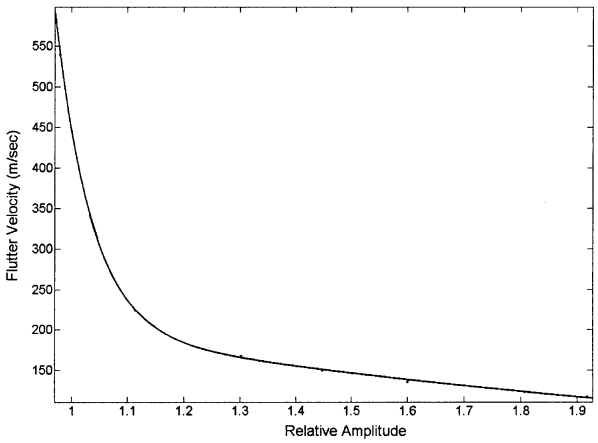

Fig.10 Variation of Flutter Velocity with Relative Amplitude